2020 IEEE International Conference on Robotics and Automation (ICRA)
31 May - 31 August, 2020. Paris, France

A Variable Stiffness Soft Continuum Robot Based on Pre-charged Air, Particle Jamming, and Origami

Yujia Li, Tao Ren, Yonghua Chen, *Member, IEEE*, and Michael Z. Q. Chen, *Senior Member, IEEE*

***Abstract*—Soft continuum robots have many applications such as medical surgeries, service industries, rescue tasks, and underwater exploration. Flexibility and good accessibility of such robots are the key reasons for their popularity. However, the complexity of their structural design and control systems limit their broader applications. In this paper, a novel variable stiffness soft continuum robot based on pre-charged air, particle jamming, and origami is proposed. The robot is a bellow-like origami structure with internal chambers. A spine-like chamber is filled with particles, and three identical chambers surrounding the spine chamber are filled with pressurized air. When the origami structure is compressed, the particles are jammed by the compression force and the increased pressure of the three air chambers, thus increasing the overall stiffness of the robot. The robot expansion-contraction and bending are controlled by three tendons. An analytical model of the proposed stiffness variation mechanism has been developed. The effects of various parameters on the lateral and axial stiffness of the soft continuum robot have been investigated by experimental studies. A prototype robot has been fabricated to demonstrate grasping operations.**

***Index Terms*—Soft continuum robot, variable stiffness, pre-charged air, particle jamming, origami**

I. Introduction

Several methods for soft robot and continuum robot actuation have been used in various configurations and different working environments [1]. These methods include pneumatics [2,3], electroactive polymers [4,5], shape memory alloys [6], electro-rheological and magneto-rheological fluids [7], and cable-driven approaches [8]. Many studies on pneumatic methods have been conducted due to their early development and simple principle. Pneumatic methods use gas pressure differentials to deform flexible structures to achieve certain motions and functions [9,10]. However, most pneumatic soft actuators require heavy air compressors and valves, and several hoses are connected between the air compressor and the robot, thus limiting the flexibility and range of motion of the soft continuum robots. Cable-driven method makes soft continuum robots miniaturized [11-13]. But it's hard to change the stiffness of the cable-driven soft continuum robots.

An increasing number of soft robots must have variable stiffness to adapt to changes in complex environments, such as soft/hard, light/heavy, and big/small objects. Robotic arms/hands must have flexible compliance with the body and the necessary stiffness modulation capability [14]. Several approaches of variable stiffness based on different technologies, such as variable-rigidity materials [15], electric [16] and magnetic field-induced [17], and thermal [18] and pressure-induced methods [19, 20], are available. The pressure-induced control is widely studied because it is simple, fast, and effective. At present, most research and applications are based on vacuuming a particle pack from flowing to jamming states to achieve variable stiffness. However, this method requires a heavy vacuum pump, hoses, and valves, while such components are bulky and inconvenient, limiting the scope of applications.

Based on the aforementioned issues, the authors conducted a series of studies in the early stage to develop new structures and principles of soft robots [17-24]. The soft pneumatic actuator and variable stiffness configuration are reduced as much as possible to suit a variety of applications. Based on previous research, this paper proposes a new method for stiffness modulation based on particle jamming. Instead of using a vacuum, the proposed method generates a jamming effect by actively controlling the air pressure around the particle pack by tendons and a compressible origami structure.

The major contributions of this research are presented in three aspects. First, a novel variable stiffness soft continuum robot based on pre-charged air, particle jamming, and origami structure is proposed. Second, the analytic model of the proposed soft continuum robot is established. Finally, the effect of particle size, air pressure (difference), and continuum robot structural parameters on its stiffness is investigated in the experiments. The potential applications of the soft continuum robot are demonstrated.

II. Basic Design and Fabrication

The variable stiffness soft continuum robot comprises a bellow-like origami structure, as shown in Fig. 1(a). The inner part of the origami structure is designed as a hollow three-lobed structure as in Fig. 1(b) to have adequate stiffness. The hollow space of the three-lobed structure is filled with particles. A wire guide structure is designed on each of the lobes. The particle-filled three-lobed structure serves as the spine of the soft continuum robot. The three air chambers are filled with pressurized air and sealed before actual operations.

This work was supported by National Natural Science Foundation of China (NSFC) under Project 51805443, Sichuan Science and Technology Program under Project 2019YFG0123, and Young Scholar of Xihua University.

Yujia Li is with the School of Mechatronic Engineering, Southwest Petroleum University, Chengdu 610500, China (e-mail: yujiali321@foxmail.com).

Tao Ren is with the Robotics Research Center, Xihua University, Chengdu 610039, China (Corresponding author, e-mail: rtone@foxmail.com).

Yonghua Chen is with the Department of Mechanical Engineering, The University of Hong Kong, Pok Fu Lam, Hong Kong (e-mail: yhchen@hku.hk).

Michael Z. Q. Chen is with the School of Automation, Nanjing University of Science and Technology, Nanjing 210094, China (e-mail: mzqchen@outlook.com).

For the prototype in this research, the origami structure has a length of 210 mm and an outer contour diameter of 48 mm; the wall thickness is 0.6 mm. The inner cylinder is a three-lobed hollow bellow structure. The spacing between every two layers of corrugation is 7 mm. The bellow structure is designed to reduce the internal volume linearly when the length of the structure is shortened. This process will lead to reduced volume of the air chambers, which increases their air pressure, resulting in particle jamming or stiffness increase in the soft continuum robot. The outer rings are connected by a tendon guide every 35 mm. The entire structure is fabricated in one piece by 3D printing using thermoplastic polyurethane (TPU) materials. The printer head has a diameter of 0.4 mm. The printer parameters are set to 0.2 mm per layer thickness and 30% filling density.

Three type-304 stainless steel wires with a diameter of 0.5 mm passing through the tendon guide are used to control the contraction and bending of the soft continuum robot. This type of steel wire is used for its stiffness. Thus, the length variation factor of the actuating tendon itself can be excluded in the experimental test. The cable-driven design facilitates linear control of continuum robot deformation, reducing the complexity of the pneumatic control valve system.

When the actuation tendon is shortened, the radial dimension is constant and the axial dimension is reduced. These conditions decrease the volume of the three-lobed particle-filled structure and that of the three air chambers. Thus, the particles will change from flowing to jamming states, increasing the rigidity of the entire continuum robot. In this study, the tendons serve multiple purposes: positional and stiffness control. Compared with conventional vacuum-based particle jamming, the proposed method avoids the use of vacuum pumps, air tubes, and complex valve controls.

Owing to possible air leakage in the 3D-printed air chambers inside the soft continuum robot, three elastic latex tubes with an outer diameter of 17 mm and thickness of 1.5 mm were placed inside the chambers to serve as air chambers as shown in Fig. 1(c). One end of the latex tube is sealed with a sealing head and a clamp. The other end is connected to the air tube and the check valve (serves the same function as the basketball valve) to pre-charge the latex tube to the desired air pressure. When the actuation tendon is shortened, the length of the air chamber is reduced, and the air pressure and the stiffness of the robot are increased. The pre-charged air chamber design avoids the use of heavy air compressors, valves, and long air tubes, making the soft continuum robot transportable. Furthermore, the pre-charged structure can increase the initial stiffness of the robot for centering. The three air chambers can be pre-charged to compress the particles inside the spine to prevent initial particle flow. The pre-bending effect of the robot can be achieved if the pre-charged pressures in the three air chambers are different. Thus, the robot can be linearly driven by wires. This principle is similar to the concept of pre-charged pneumatics previously reported by the authors' team [23].

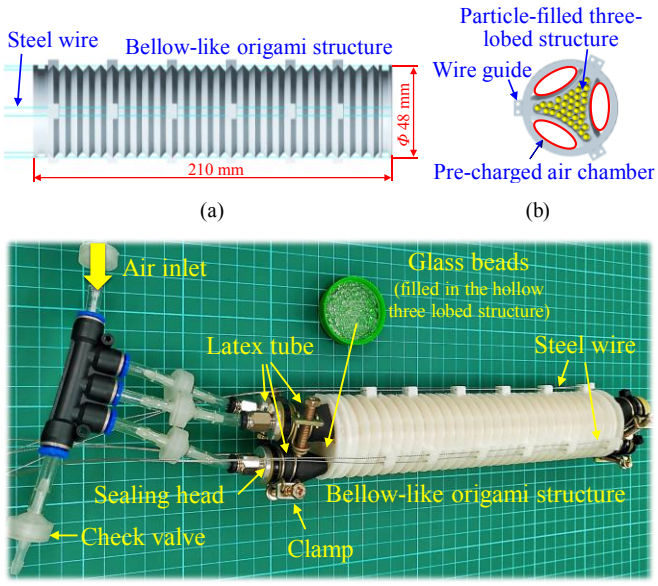

Figure 1. Basic design concept. (a) The bellow-like origami structure. (b) A cross-section showing the three-lobed structure filled with particles and three air chambers. (c) A prototype.

III. Modeling and Analysis

The deformation of the continuum robot is achieved by pulling the wire. The displacement of the wire also determines the change in air pressure of the air chambers. When the pre-charged air chambers are compressed by the axial force, the elastic latex tube is squeezed to expand laterally, as shown in Fig. 2(b). Lateral expansion causes the latex tube to produce a laterally uniform load that squeezes the particle spine. The axial force F due to tendon pulling also contributes to compression of the particle spine, as shown in Fig. 2(c).

Given that the inner particle-filled three-lobed structure and the outer origami structure are corrugated, the inner latex tube is radially expanded after compression of the elastic chamber, conforming to the corrugated surface and pressing the particle spine. The cross-sectional area of the latex tube is calculated based on the area formula of an ellipse. For the convenience of calculation, the average value of the maximum and minimum areas of the ellipse between the inner three-lobed bellow structure and the outer bellow-like origami structure is taken as the sectional area of the pressurized air chamber. Based on the ideal gas state equation,

$$P_1V_1 = P_2V_2 = nRT\,. \tag{1}$$

The air pressure in the air chamber after compression is

$$P_2 = \frac{P_1V_1}{V_1 - \pi ab\Delta L} = q(y)\,, \tag{2}$$

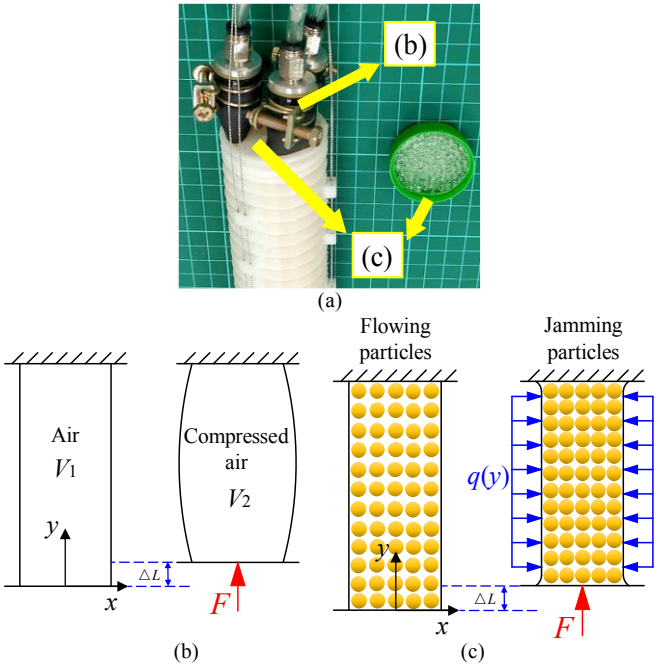

Figure 2. Working principle of the particle jamming pressure change. (a) Diagram of the air and particle chambers. (b) Air chamber compression. (c) Particle chamber compressed by tendon pulling force F and air pressure from three chambers.

where P_1 and V_1 are the initial air pressure and volume of the air chamber, respectively; P_2 and V_2 are the air pressure and volume of the compressed air chamber, respectively; n is the amount of gas substance; R is the ideal gas constant; T is the thermodynamic temperature of the ideal gas; a and b are the major and the minor axes of the elliptical section of the gas chamber, respectively; and ΔL is the length change of the gas chamber or the soft continuum robot.

The compressed air pressure P_2 acts as a distributed load $q(y)$ on the particle spine and cooperates with the pulling force F to squeeze the particles in the particle spine to change its stiffness. A large pulling force results in a large length change ΔL. Thus, the stiffness of the continuum robot is also high.

IV. Experimental Studies

The structure of the variable stiffness soft continuum robot is a bellow-like origami structure with internal pre-charged air and particle chambers (which serve as a spine). The lateral and axial stiffness of the continuum robot are investigated considering the effects of various parameters. In addition, a potential application of the variable stiffness soft continuum robot is presented by grasping demonstrations.

A. Experimental Tests of Variable Stiffness

An experimental test platform is established as shown in Fig. 3. The soft continuum robot is fixed vertically on a wooden board against the wall, in which one end is fixed and the other end is suspended. A square piece of paper with a spacing of 10 mm per line is attached to the board to observe the lateral and axial displacements and the bending angle of the continuum robot. Two motor-driven screw linear guides are set in the horizontal and vertical directions. Force sensors 1 and 2 are driven by the two linear guides to pull the continuum robot and record the pulling force. All the experiments were

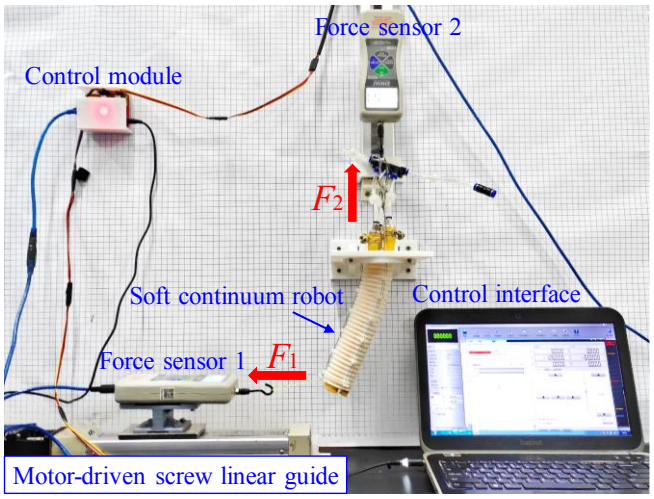

Figure 3. Stiffness test platform.

performed at room temperature at least three times to ensure repeatability. The average values are obtained, and the experimental results are plotted in Figs. 4 to 6. The standard deviations are not shown in the figures because the experimental error, from approximately 0 to 0.02, is extremely small relative to the pulling force.

(1) Lateral Stiffness

The soft continuum robot is shortened by pulling the three actuation tendons with the motor-driven screw linear guide. One end of the continuum robot and force sensor 1 is connected with a Kevlar line. The linear guide drives the force sensor 1 to move toward the left by 50 mm at a speed of 60 mm/min. The values of the force during the pulling process are recorded. The effect of the particle diameter and pre-charged air pressure on the lateral stiffness of the continuum robot at different lengths was tested in the experiments. The particulate material used in the experiment is glass beads. The pre-charged pressures of the three air chambers are equal. The experimental results are shown in Fig. 4. The ΔL indicated in the figure is the shortened length of the soft continuum robot, D is the particle diameter, and P is the pre-charged air pressure.

The lateral force tends to increase linearly with the lateral pulling displacement and the pre-charged air pressure. This finding indicates that the lateral stiffness of the continuum robot increases with the pre-charged air pressure. The reason is that the pre-tightening force of the particles in the three-lobed bellow structure is increased after the pressure, further preventing the occurrence of flow and facilitating the possible change of particles to a jamming state. Furthermore, the air pressure is increased to resist deformation. Therefore, the lateral stiffness of the continuum robot is increased.

The lateral pulling force slightly differs when the particle diameter is 1 and 2 mm. When the particle diameter is increased to 3 mm, the lateral pulling force tends to decrease. This condition indicates that the lateral stiffness of the continuum robot is large when the particle diameter is small because the contact area between every two particles increases as the diameter of the particles decreases. Therefore, the

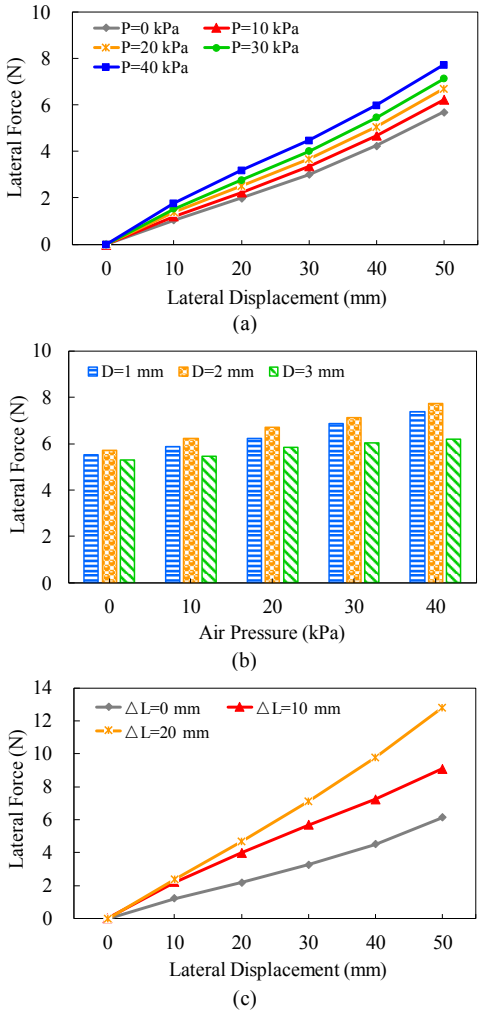

Figure 4. Lateral stiffness tests. (a) ΔL = 0 mm; D = 2 mm; P = 0, 10, 20, 30, 40 kPa. (b) ΔL = 0 mm; D = 1, 2, 3 mm; P = 0, 10, 20, 30, 40 kPa. (c) ΔL = 0, 10, 20 mm; D = 2 mm; P = 20 kPa.

number of strong chains in the particles increases, resulting in an enhanced effect against external action and resistance to deformation; thus, lateral stiffness is enhanced [21]. In addition, the lateral pulling force and stiffness tend to increase considerably as the length of the continuum robot decreases.

A comparative experiment is conducted to further test the influence of the air pressure difference of the three air chambers and the distribution of the soft continuum robot structure on the lateral stiffness. The steel wire was removed in this experiment to eliminate the influence of the steel wire on the structure. As shown in Fig. 5(a), the pre-charged pressures of air chambers 1 and 2 are equal to 40 kPa. The air chamber 3 pressures are 0, 10, 20, 30, and 40 kPa. Lateral pulling force is applied with the displacement of 50 mm as shown in Fig. 3. The experimental results show that a large pre-charged pressure difference of the three air chambers leads to a small lateral pulling force and low stiffness. Thus, the lateral stiffness of the continuum robot can be changed by varying the air pressure difference between the three chambers.

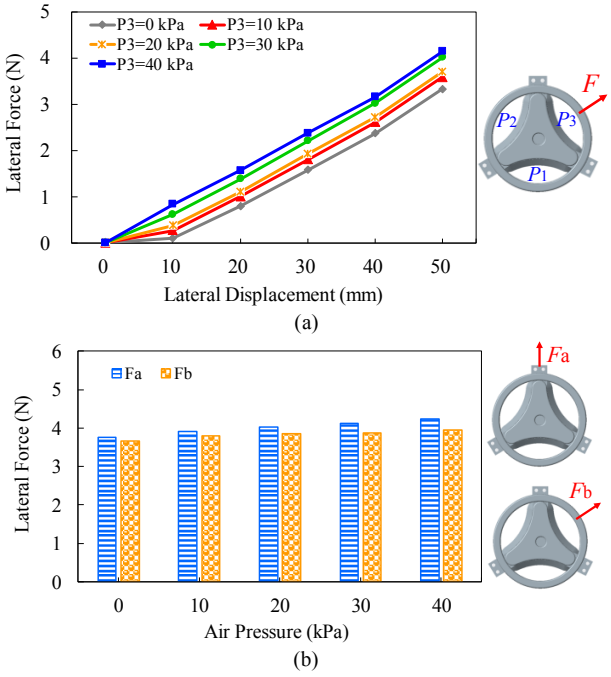

Figure 5. Lateral stiffness tests. (a) ΔL = 0 mm; D = 2 mm; P1 = P2 = 40 kPa; P3 = 0, 10, 20, 30, 40 kPa. (b) ΔL = 0 mm; D = 2 mm; P1 = P2 = P3 = 0, 10, 20, 30, 40 kPa.

As shown in Fig. 5(b), the pre-charged pressures of the three air chambers are equal. The lateral pulling force is applied from both directions with the displacement of 50 mm.

The experiment shows that the structural distribution of the robot has a slight effect on the lateral stiffness. The lateral pulling force in the F_a direction is slightly larger than that of the F_b direction; that is, the lateral stiffness in the F_a direction is slightly larger than that of the F_b direction.

(2) Axial Stiffness

The pre-charged air pressures of the three air chambers are settled equally. The three actuation tendons are pulled using a motor-driven screw linear guide to shorten the continuum robot by 20 mm. The value of force sensor 2 is continuously recorded during the pulling process.

As shown in Fig. 6(a), a short length of the continuum robot leads to a large pre-charged air pressure of the three air chambers, resulting in a large axial pulling force and high axial stiffness. The internal air chambers and particles are compressed when the length of the soft continuum robot is shortened. The air pressures in the air chambers are increased, and the deformation resistance is enhanced. Moreover, the particles vary from flowing to jamming states. These factors work together to increase the axial stiffness of the continuum robot.

As shown in Fig. 6(b), as the diameter of the particles increases, the axial pulling force first increases and then decreases. The axial force reduction of the particles with a diameter of 3 mm is also remarkable. These results correspond to those presented in Fig. 4(b). The particles with a diameter of 2 mm are matched to the size of the continuum robot designed

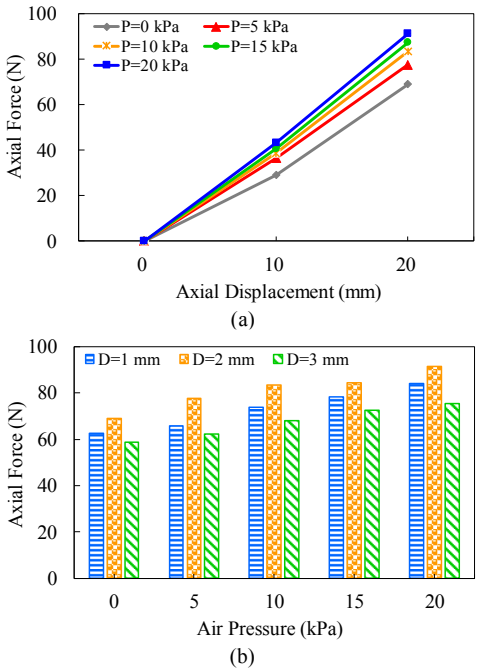

Figure 6. Axial stiffness tests. (a) ΔL = 0, 10, 20 mm; D = 2 mm; P = 0, 5, 10, 15, 20 kPa. (b) ΔL = 20 mm; D = 1, 2, 3 mm; P = 0, 5, 10, 15, 20 kPa.

in this paper, making it prone to jamming. Furthermore, the effect of stiffness enhancement is evident.

The air pressure test platform in Fig. 7 is established to monitor the air pressure change during the stiffness variation of the continuum robot to further understand the change of stiffness. The pressure sensor (3000 series pressure sensor produced by Hong Kong North ZTT) is connected to three air chambers. The voltage value of the pressure sensor is read and recorded during the contracting process of the continuum robot. Therefore, the corresponding air pressure value can be obtained. The experimental results show that the gas pressure in the gas chamber increases approximately linearly during the contraction of the continuum robot. The air pressure increased to 24.95 kPa after the continuum robot pre-charged with 20 kPa air is contracted by 20 mm. Comparing the calculation results in the modeling, the calculated air pressure increases to 23.88 kPa by using Eq. (2). The relative error is approximately 4%.

In the aforementioned experiment, the lateral and axial pulling forces linearly increase with the displacement of the wire. The cause of this phenomenon is also analyzed. The uniaxial pressure experiments of glass beads were conducted in the previous research of the authors. Initially, the force increases linearly with the compression displacement. The force rapidly decreased when it reaches a peak, indicating that the glass beads in the steel container are cracked or crushed [21]. Therefore, the particles exhibit elastic deformation characteristics before they are crushed.

A DS2-100N dynamometer produced by ZHIQU Precision Instruments Co., Ltd. is used in the experiment. The range of the dynamometer is 0 N to 100 N. This dynamometer can only test the contracting force of the continuum robot by 20 mm, which is far less than that of crushing the particles.

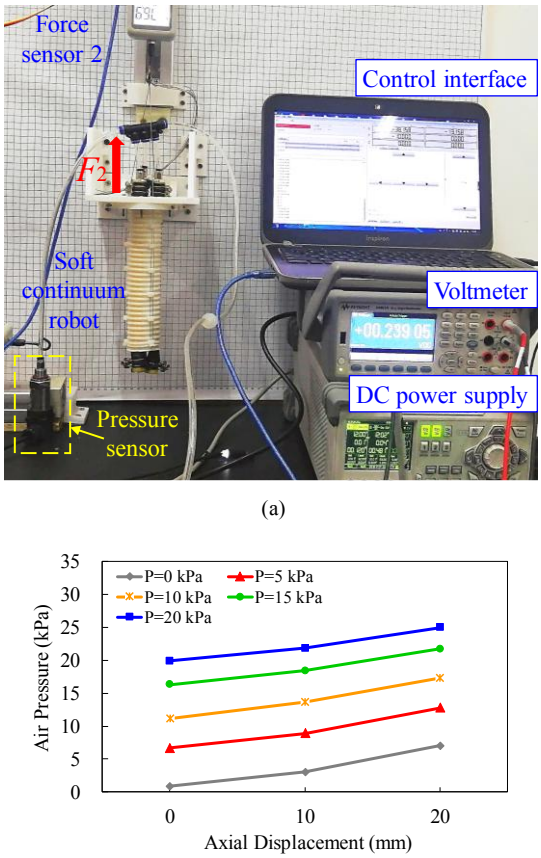

Figure 7. Air pressure changes at different axial displacements and initial pre-charged air pressures. (a) Air pressure test platform. (b) Air pressure test results.

Therefore, the relationship between force and displacement in this experiment is linear, indicating that the particles have certain compressibility. When compressing the chambers filled with particles within a certain force range, the external pulling force breaks the balance between the particles, causing the slippage or rotation of some particles. The contact between the particles is unstable, causing the breakage and recombination of force chains between the particles, which, in turn, facilitates the solid-liquid transition of the particles. When the force is increased to a certain value, the porosity of the particle system is minimized and the structural rigidity reaches its maximum. If the force is increased afterward, then the particles will be crushed and broken.

B. Variable Stiffness and Grasping Demonstration

The proposed soft continuum robot can be used to develop advanced applications due to its variable stiffness, linear control, and portability. A grasping experimental platform based on the variable stiffness soft continuum robot is designed and fabricated in this study, as shown in Fig. 8. The continuum robot is fixed on a support. The support is fixed on the test bench constructed using aluminum. A soft gripper based on compliant mechanisms is attached to the end of the continuum robot by a 3D-printed bracket. The soft gripper comprises TPU materials by 3D printing, and the printing

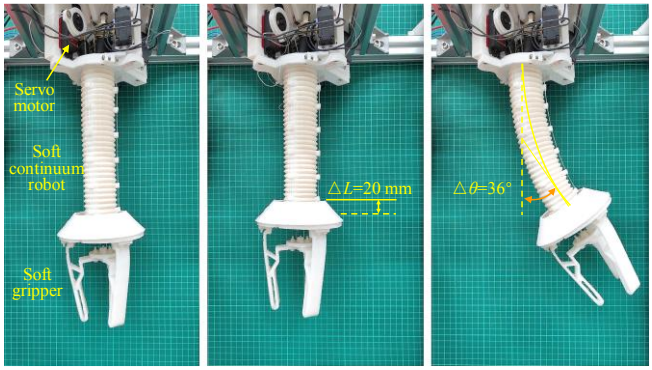

Figure 8. Soft continuum robot moving range.

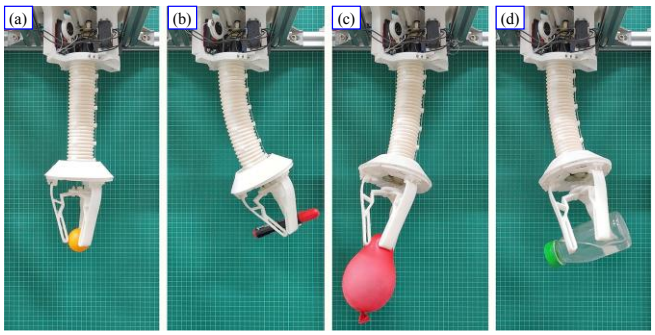

Figure 9. Demonstration of sample grasping. (a) Table tennis ball (2.85 g). (b) Pen (16.76 g). (c) Balloon (1.06 g). (d) Water-filled bottle (162.45 g).

parameters are the same as those of the bellow-like origami structure.

Three nylon threads are used as the actuation tendons, which are wound around three reels. Three servo motors control the rotational angles of the three reels to change the length of the actuation tendon, thereby controlling the motion of the continuum robot. One end of a nylon thread is tied to the palm of the soft gripper, and the other end is wrapped around a reel. The opening and closing of the soft gripper is controlled by a servo motor. The battery can be installed on the continuum robot in remote jobs. The continuum robot can be shortened by up to 20 mm, and the maximum bending angle is 36° (which is limited by the current servo motion range in the prototype; the servos by servo motors will be replaced to expand the bending range and controllability in our coming development).

In the grasping demonstration experiment presented in Fig. 9, objects with a range of different features, such as a table tennis ball, a pen, a balloon, and a water-filled bottle, were tested. Experimental results show that the variable stiffness soft continuum robot can be combined with a soft gripper to capture soft/hard and light/heavy objects. This experiment demonstrates the application possibilities of the continuum robot in the gripper and bionic muscle.

V. Conclusion and Discussion

This article presented a novel variable stiffness soft continuum robot, which has many advantages over conventional soft continuum robot. First, the stiffness of particles remarkably increases under the combined action of tension wire and air pressure. Second, the pre-charged air chamber design avoids the use of heavy air compressors, valves, and considerably long air tubes, making the robot transportable. Third, the structural volume of variable stiffness by compressing the particle chamber is smaller than that of the conventional particle vacuum structure, decreasing the need for air tightness of the origami structure. Fourth, the design of pulling wire enables the easy linear control of the stiffness of the continuum robot, reducing the complexity of the control system. Finally, the foldable bellow-like structural design enables the soft continuum robot to produce large expansion-contraction and continuous uniform bending deformations, preventing buckling when the wire is pulled (The wire guides are designed at the three particle lobes).

The lateral and axial stiffness have been experimentally studied. The experimental results show that the lateral stiffness tends to increase linearly with the pre-charged air pressure, the decrease in the continuum robot length, and the reduction in the pre-charged pressure difference of the three air chambers. Particle diameter and structural symmetry have slight effects on lateral stiffness. The axial stiffness tends to increase linearly with the decrease in the continuum robot length and the increase in the pre-charged air pressure of the three chambers. As the diameter of the particles increases, the axial stiffness first increases and then decreases. This result helps to optimize the design of the continuum robot based on functional requirements. Finally, the potential application of the continuum robot in the gripper and bionic muscle is presented by the grasping demonstration.

In the future work, the authors are aiming to develop a continuum robot with more modules, similar to the prototype shown in this paper. This will allow more degrees of freedom. Furthermore, the control algorithm can be optimized according to the environmental characteristics, so that the soft continuum robot can handle more complex tasks.

References

[1] A. Miriyev, K. Stack and H. Lipson, "Soft material for soft actuators," *Nature Communications*, vol. 8, no. 1, pp. 596, December 2017.

[2] Y. Wang, X. Yang, Y. Chen, D. K. Wainwright, C. P. Kenaley, Z. Gong, Z. Liu, H. Liu, J. Guan, T. Wang, J. C. Weaver, R. J. Wood and L.Wen, "A biorobotic adhesive disc for underwater hitchhiking inspired by the remora suckerfish," *Science Robotics*, vol. 2, no. 10, pp. eaan8072, September 2017.

[3] H. Zhao, K. O'Brien, S. Li and R. F. Shepherd, "Optoelectronically innervated soft prosthetic hand via stretchable optical waveguides," *Science Robotics*, vol. 1, no. 1, pp. eaai7529, December 2016.

[4] G. Gu, J. Zou, R. Zhao, X. Zhao and X. Zhu, "Soft wall-climbing robots," *Science Robotics*, vol. 3, no. 25, pp. eaat2874, December 2018.

[5] T. Li, G. Li, Y. Liang, T. Cheng, J. Dai, X. Yang, B. Liu, Z. Zeng, Z. Huang, Y. Luo, T. Xie and W. Yang, "Fast-moving soft electronic fish," *Science Advances*, vol. 3, no. 4, pp. e1602045, April 2017.

[6] S. Seok, C. D. Onal, K. J. Cho, R. J. Wood, D. Rus and S. Kim, "Meshworm: A peristaltic soft robot with antagonistic nickel titanium coil

actuators," *IEEE/ASME Transactions on Mechatronics*, vol. 18, no. 5, pp. 1485-1497, October 2013.

[7] S. Kashima, F. Miyasaka and K. Hirata, "Novel soft actuator using magnetorheological elastomer," *IEEE Transactions on Magnetics*, vol. 48, no. 4, pp. 1649-1652, April 2012.

[8] H. Wang, C. Wang, W. Chen and X. Liang, "Three-dimensional dynamics for cable-driven soft manipulator," *IEEE/ASME Transactions on Mechatronics*, vol. 22, no. 1, pp. 18-28, September 2016.

[9] F. Wyatt, M. J. Telleria, T. F. Allen, H. Gabriel, J. B. Pompa and A.Kevin, "An inductance-based sensing system for bellows-driven continuum joints in soft robots," *Autonomous Robots*, vol. 43, pp. 435–448, February 2019.

[10] A. Grzesiak, R. Becker and A. Verl, "The bionic handling assistant: a success story of additive manufacturing," *Assembly Automation*, vol. 31, no. 4, pp. 329-333, September 2011.

[11] W. McMahan, B. A. Jones and I. D. Walker, "Design and implementation of a multi-section continuum robot: Air-Octor," *IEEE/RSJ International Conference on Intelligent Robots and Systems*, pp. 2578-2585, August 2005.

[12] R. Cieślak, A. Morecki, "Elephant trunk type elastic manipulator-a tool for bulk and liquid materials transportation," *Robotica*, vol. 17, no. 1, pp. 11-16, January 1999.

[13] G. Immega and K.Antonelli, "The KSI tentacle manipulator," *IEEE International Conference on Robotics and Automation*, Vol. 3, pp. 3149-3154, May 1995.

[14] L. Wang, Y. Yang, Y. Chen, C. Majidi, F. Iida, E. Askounis and Q. Pei, "Controllable and reversible tuning of material rigidity for robot applications," *Materials Today*, vol. 21, no. 5, pp. 563-76, June 2018.

[15] I. Kuder, A. Arrieta, W. Raither and P. Ermanni, "Variable stiffness material and structure concepts formorphing applications," *Progress in Aerospace Sciences*, vol. 63, no. 2013, pp. 33-55, November 2013.

[16] A. Tonazzini, A. Sadeghi and B. Mazzolai, "Electrorheological valves for flexible fluidic actuators," *Soft Robotics*, vol. 3, no. 1, pp. 34-41, March 2016.

[17] M. Zeng, Y. J. Li, T. Ren and Q. Tu, "Material stiffness control of compliant tools by using electromagnetic suction," *Proceedings of the Institution of Mechanical Engineers, Part C: Journal of Mechanical Engineering Science*, vol. 233, no. 13, pp. 4719-4728, February 2019.

[18] Y. Yang, Y. H. Chen, Y. T. Li, Wang Z and Y. Q. Li, "Novel variable-stiffness robotic fingers with built-in position feedback." *Soft Robotics*, vol. 4, no. 4, pp. 338-52, June 2017.

[19] Y. Li, Y. Chen, Y. Yang and Y Wei, "Passive particle jamming and its stiffening of soft robotic grippers," *IEEE Transactions on Robotics*, vol. 33, no. 2, pp. 446-55, January 2017.

[20] N. G. Cheng, M. B. Lobovsky, S. J. Keating, A. M. Setapen, K. I. Gero, A. E. Hosoi and K. D. Iagnemma, "Design and analysis of a robust, low-cost, highly articulated manipulator enabled by jamming of granular media," I*EEE International Conference on Robotics and Automation*, pp. 4328-4333, May 2012.

[21] Y. Li, T. Ren, Y. Li and Y. Chen. "Small-beads Transmission and Its Application to Robot Joints, " *IEEE/ASME Transactions on Mechatronics*, 2019, 24(5): 2282-2292.

[22] Y. Li, Y. Chen and Y. Li, "Pre-charged pneumatic soft gripper with closed-loop control, " *IEEE Robotics and Automation Letters*, vol. 4, no. 2, pp. 1402-1408, April 2019.

[23] Y. Q. Li, Y. H. Chen, T. Ren, Y. L. Li and S. H. Choi, "Precharged pneumatic soft actuators and their applications to untethered soft robots," *Soft Robotics*, vol. 5, no. 5, pp. 567-575, June 2018.

[24] Y. Wei, Y. H. Chen, T. Ren, Q. Chen, C. X. Yan, Y. Yang and Y. T. Li, "A novel, variable stiffness robotic gripper based on integrated soft actuating and particle jamming," *Soft Robotics*, vol. 3, no. 3, pp. 134-143, July 2016.